Three-Dimensional Analysis of Complex Anisotropic Slope Instability at MMG's Century Mine

D. P. Sainsbury, B. L. Sainsbury and E. Sweeney

Anisotropic and foliated rock masses present particular difficulties in the assessment of pit slope stability. Although many attempts have been made to describe the strength of rock masses that exhibit a preferred orientation of weakness, no general methodology has emerged throughout the literature to simulate anisotropic behaviour in a three-dimensional numerical model of pit slope stability. In order to simulate the effect of the anisotropic shale rock mass on pit slope stability at MMG Limited's (MMG) Century Mine, the Ubiquitous Joint Rock Mass (UJRM) method developed by Sainsbury and Sainsbury (2013) has been applied. This paper outlines the methodology that was used to assist mine personnel in the management of complex anisotropic slope instability that jeopardised the recovery of 1.8 Million tonnes of zinc ore.

1. Introduction

The Century Mine is located approximately 250 km's north-west of Mount Isa, close to the Northern Territory border in Far North Queensland, Australia. For the majority of its life, the mine has been the largest producer of zinc in Australia and the third largest in the world producing approximately 500,000 tonnes of zinc concentrate annually (Sweeney and Abbott, 2015).

The open pit zinc mine has been developed in a series of cutbacks to a depth of approximately 350 m. Figure 1 illustrates a plan view of the open pit at May 2013 with the various active cutbacks.

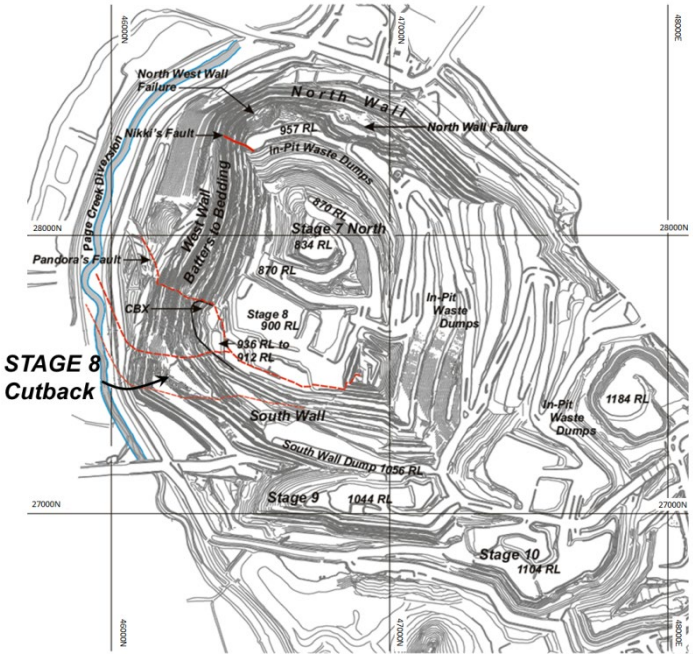

Figure 1 Plan view of Century Mine, May 2013

During excavation of the Stage 8 Cutback from 2010 to 2014, significant slope instability evolved within the highly anisotropic shale rock mass which jeopardised the recovery of 1.8 millions of tonnes of ore. To safely and efficiently extract the remaining ore beneath the unstable area, it was critical to develop a thorough understanding of the geotechnical conditions and failure mechanisms which could be communicated and managed to reduce both the likelihood and consequences of the progressive slope failure to an acceptable level of risk. Advanced numerical modelling provides a tool to calibrate complex slope failure mechanisms and predict the response of the slope after additional excavation.

In order to accurately simulate the observed failure mechanism, a three-dimensional numerical modelling technique that can simulate the anisotropic rock mass strength and deformation behaviour of the shale rock mass, together with the effect of large-scale discrete geological structures was required. The Ubiquitous Joint Rock Mass (UJRM) modelling technique developed by Sainsbury *et al.*, (2008) and Sainsbury and Sainsbury (2013) was implemented to analyse the Stage 8 Cutback instability.

In conjunction with various forms of characterisation, analysis and monitoring (Kurucuk and Sweeney, 2012; Sweeney and Abbott, 2015; Salvoni *et al.*, 2015a; Salvoni *et al.*, 2015b), the modelling results presented herein assisted mine personnel implement a management plan that allowed successful recovery of the ore that was deemed at risk.

2. Background

2.1. Geotechnical Conditions

The West Wall at the MMG Century Mine is characterised with two distinct geomechanical domains; the Upper Footwall Shale (UFWS) and the Lower Footwall Shale (LFWS). The LFWS is dominated by black carbonaceous shales, a tight and fair rock mass with distinctive bedding. In comparison, the UFWS comprises black laminated shales, a more competent rock mass with distinctive laminated bedding (Hendersonhall *et al.*, 2010). Strong strength anisotropy due to bedding partings is observed in both of these domains as shown in Figure 2.

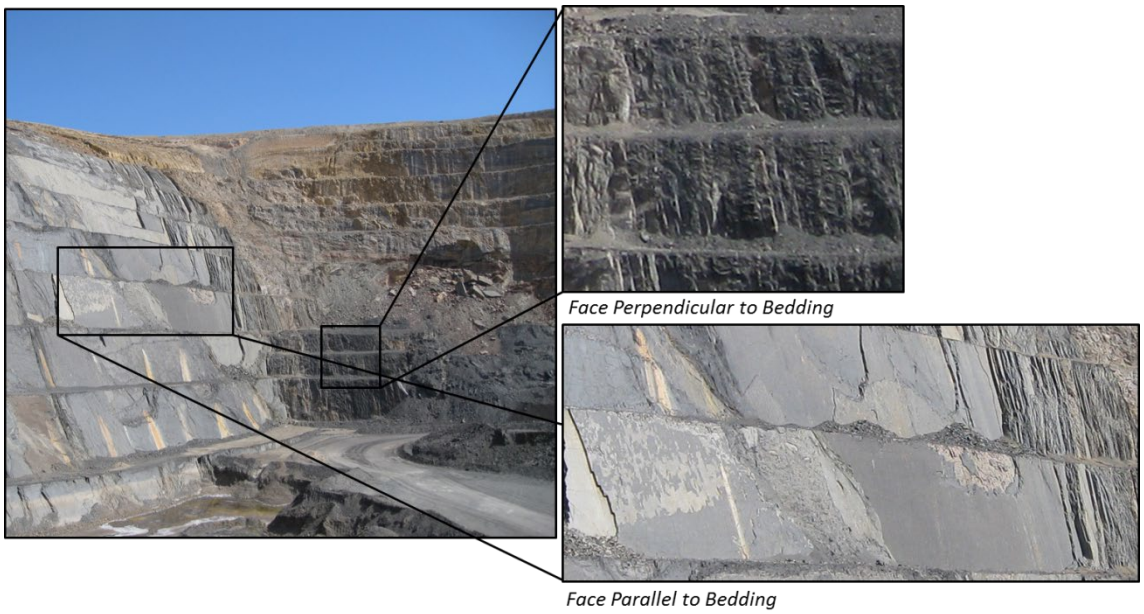

Figure 2 **Anisotropic rock mass domains and existing conditions in the West Wall at the MMG Century Mine**

Pandora's fault, a deposit scale major structure, represents the boundary between these two domains. It is a gently to moderately north dipping, EW striking normal fault, which

displaces the ore body into two major blocks. It has been interpreted as a scissor fault, with displacement varying along the strike from zero at the eastern margin of the deposit to over 300 m at the western margin (Broadbent *et al.*, 2002). Along this fault, a massive block of intrusive Carbonate Breccia (CBX) outcrops.

In the SW corner of the Stage 8 Cutback, Pandora's Fault displays a sharp change in orientation from a strike of EW to NW. The area is also characterised by the presence of a set of EW striking, north dipping, sub-vertical structures. One of those structures, known as Page Creek Fault, has contributed to the local rotation of bedding and joint features, resulting in the formation of a highly sheared and fractured block (Kurukuk and Sweeney, 2012).

2.2. Stage 8 Cutback Instability

Significant instability issues in the Stage 8 Cutback began to emerge in 2010 during excavation of the first three, 12 m benches. Wedge and planar failures emerged consistently along Page Creek Fault, which intercepted continuous, undulating bedding planes, oriented within 20° of the strike of the pit slope.

Sweeney and Abbott (2015) report that in February 2012, after two months of high rainfall, prism data began highlighted that a problem was emerging on the south and west walls. A design change was undertaken to contain a large-scale planar failure against Page Creek Fault on the South Wall. By January 2013 (in the subsequent wet season) the movement recommenced and tension cracks emerged on the West Wall in line with the strike of the shale bedding. Acceleration trends in the prism data suggested the instability was more prone to progressive movement during the wet season when pore pressure was at its peak.

Prism monitoring has indicated that the majority of the movement in the upper slope is consistent with sliding along the shale bedding planes. At the base of the slope, the prism movements indicate that the CBX block is being pushed up and out in a rotational motion as illustrated in Figure 3. The movement is generally confined between the Page Creek and Pandora's Fault which is acting as an active block, being 'retained' by a passive block of CBX. Figure 4 illustrates contours of the current prism displacements in the vicinity of the West Wall of the Stage 8 Cutback.

Based on typical slope displacement curves described by Broadbent and Zavodni (1982), the West Wall can be characterised as a Transitional System, as illustrated in Figure 5. Although significant displacement (>1 m) has occurred, to date, the Stage 8 Failure has not entered a progressive failure phase.

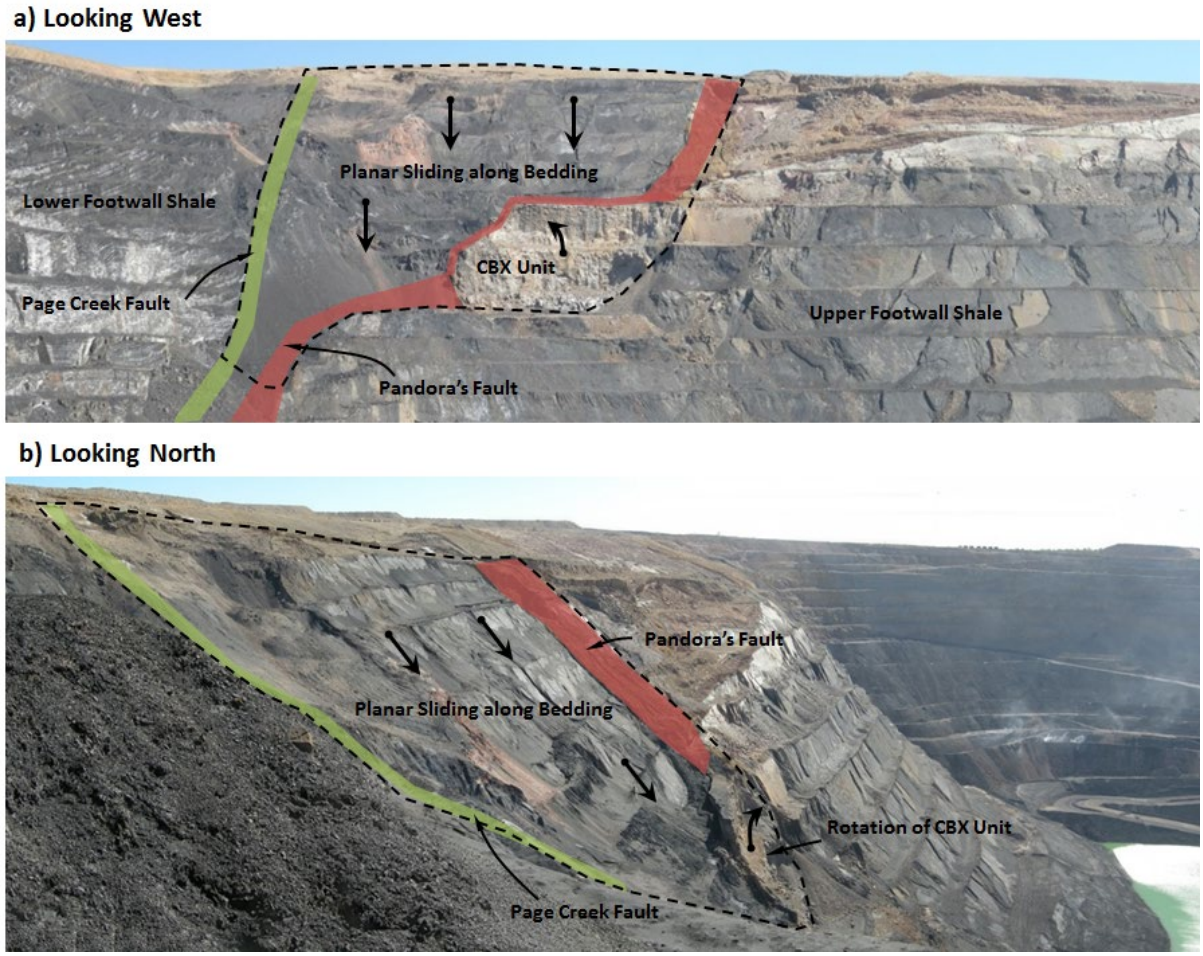

Figure 3 Conceptual model of the west wall progressive movement mechanism presented on views looking west (above) and north (below)

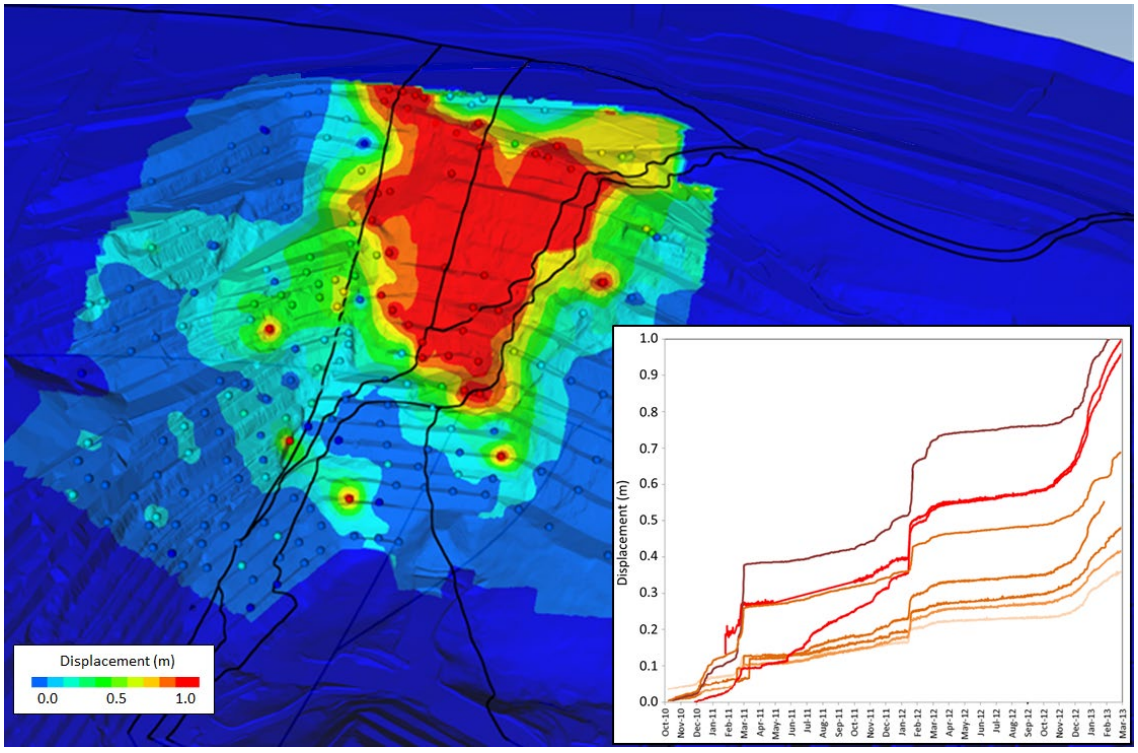

Figure 4 Contour of current measured pit slope displacement

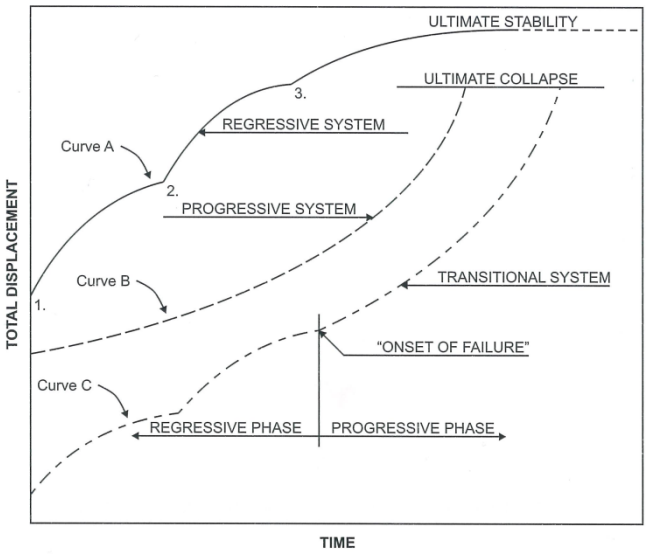

Figure 5 **Typical regressive/progressive stage displacement curves (Broadbent and Zavodni, 1982)**

3. Numerical Simulation of Anisotropic Rock Mass Strength and Deformation

The strength and deformation behaviour of a jointed rock mass is governed strongly by (a) the intact strength of the rock and (b) the presence of joints/discontinuities. When the presence of joints/discontinues align in a preferred direction, this can leaded to significant variations in strength and deformation of the rock mass depending on the direction of loading.

Although many attempts have been made in the past to describe the strength anisotropy of rock masses (Jaeger, 1960; Hoek, 1964; McLamore and Gray, 1967, Hoek and Brown, 1980 and Ramamurthy, 1993), no general methodology has emerged throughout the literature.

In order to simulate the effects of anisotropic rock mass strength and deformation behaviour on pit slope stability at the MMG Century Mine the Ubiquitous Joint Rock Mass (UJRM) modelling technique developed by Sainsbury and Sainsbury (2013) has been applied. Stead (2015) states that the UJRM modelling technique has considerable potential for future landslide and rock slope investigations in shale rock masses.

When considering the numerical analysis of anisotropic rock masses, discontinuum analysis techniques provide the most rigorous assessment of the strength and deformation behaviour. In this case, the actual joint fabric and intact rock bridges are explicitly simulated. However, due to current computational constraints, it is not possible to explicitly simulate the detailed joint fabric that controls anisotropy in large-scale, three-dimensional pit slope models. As a result, Ubiquitous Joint constitutive models are commonly used to approximate anisotropic strength and deformation behaviour in Finite-Element (FEM) and Finite-Difference (FDM) continuum models. Ubiquitous joint techniques of various forms have previously been used by Goodman (1967), Kazakidis and Diederichs (1993), Halim et al. (2008) and Clark (2006) to represent anisotropic rock mass behaviour.

The Ubiquitous Joint model corresponds to a Mohr-Coulomb continuum material that exhibits strength anisotropy due to embedded planes of weakness in each of the zones. The criterion for failure on the plane of weakness consists of a composite Mohr-Coulomb envelope with a tension cut-off. The zone-based matrix and joint properties illustrated in Figure 4 are specified for the model. The Subiquitous (Strain-Softening Ubiquitous Joint) model is a generalisation of the Ubiquitous-Joint model which allows a bi-linear Mohr-Coulomb failure envelope, together with strain-softening/hardening behaviour for both the matrix and joints. Within both the Ubiquitous and Subiquitous models, general failure is first

detected based upon the Mohr-Coulomb criteria for the matrix. Once the relevant plastic corrections are applied, the new stresses are then analysed for failure on the plane of weakness and updated accordingly. Sainsbury and Sainsbury (2013) demonstrate the ability of the UJRM technique to accurately simulate planar sliding, wedge and toppling failure mechanisms in anisotropic rock masses.

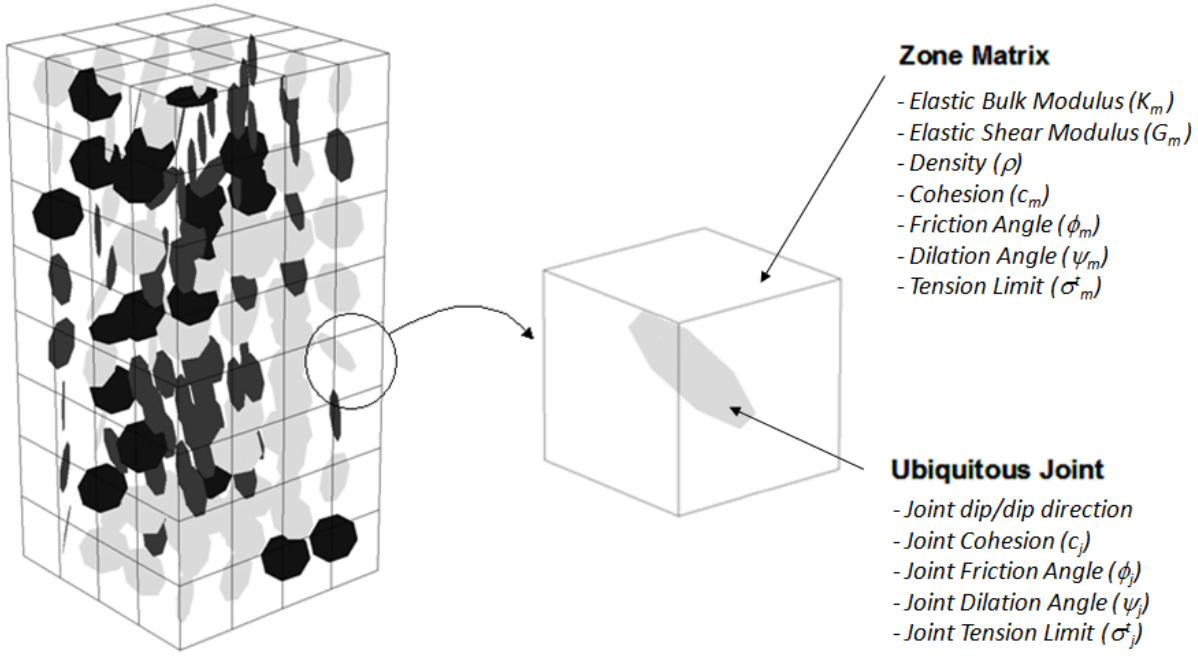

Figure 4 Zone-based matrix and ubiquitous-joint properties (after Sainsbury *et. al.*, 2008)

The ubiquitous joint formulation assumes infinitesimal spacing and no length scale to their implementation. As such, a ubiquitous-joint material cannot account for the bending stiffness of the individual layers of rock. In order to provide meaningful modelling results careful calibration of the matrix and ubiquitous joint parameters to emergent behaviour from discontinuum modelling techniques is required.

4. Geomechanical Properties

4.1. Hoek-Brown Parameters

The Hoek-Brown parameters for each of the UFWS and LFWS are summarised in Table 1. The GSI values have been calculated based on a drilling campaign. The m_i values for each of the rock mass domains have not been derived from laboratory testing, but have been estimated through empirical charts (Hoek and Brown, 1980).

Table 1 Hoek-Brown Parameters for the West Wall Rock Mass Domains

	LFWS	UFWS
UCS (MPa)	30	39
GSI	60	60
mi	6	6

4.2. Bedding Plane Shear Strength

Both the UFWS and LFWS domains at MMG Century are characterised by shales that have a bedding spacing that ranges from 20 mm to 500 mm. Bedding discontinuity strength has

been estimated based on the methodology described by Barton (1973, 1976). The values are provided in Table 2.

Table 2 Estimation of bedding discontinuity strength

	UCS (MPa)	Length (m)	Jr	JRC	JCS (MPa)	Ja	JRC_F	JCS_F (MPa)	$\phi_{j(peak)}$ (Deg.)	i (Deg.)	τ_{max} (MPa)	ϕ_b (Deg.)	Coh. (kPa)
LFWS	30	15	1.5	5	30	2.5	3	14	31	3	0.6	28	80
UFWS	39	15	1.5	5	39	2.5	3	18	31	4	0.6	28	88

4.3. In Situ Stress Regime

It was assumed that the vertical *in situ* stress is lithostatic (based on the density of the overlying rock) and the horizontal *in situ* stress magnitude is two times the vertical stress magnitude acting east-west.

5. Development of UJRM Material Properties

Numerical experiments with discontinuum modelling techniques provide significant insight and understanding of rock mechanics processes that are not possible to test in the laboratory due to specimen scale. The following sections describe the use of simulated large-scale laboratory experiments with discontinuum models under various stress paths to provide an understanding of the anisotropic strength and deformation behaviour of a particular rock mass. The emergent behaviour from the discontinuum models can then be calibrated within the Subiquitous constitutive model for use in large-scale pit slope analyses.

5.1. Discontinuum Analysis of Anisotropic Strength and Deformation Response

A series of large-scale (5 m) simulated compression tests have been conducted within the three-dimensional distinct element code *3DEC* (Itasca, 2015). To simulate the LFWS and UFWS domains, a bedding plane spacing of approximately 0.2 m – 0.5 m was assigned together with two orthogonal, non-persistent joint sets. The spacing and persistence of the joint sets was assigned to ensure the average block volume within the sample was approximately $0.1m^3$ which is consistent with a GSI of 60 after Cai *et al.,* (2007). The *3DEC* model used to simulate a representative elemental volume of the LFWS Domain is illustrated in Figure 6.

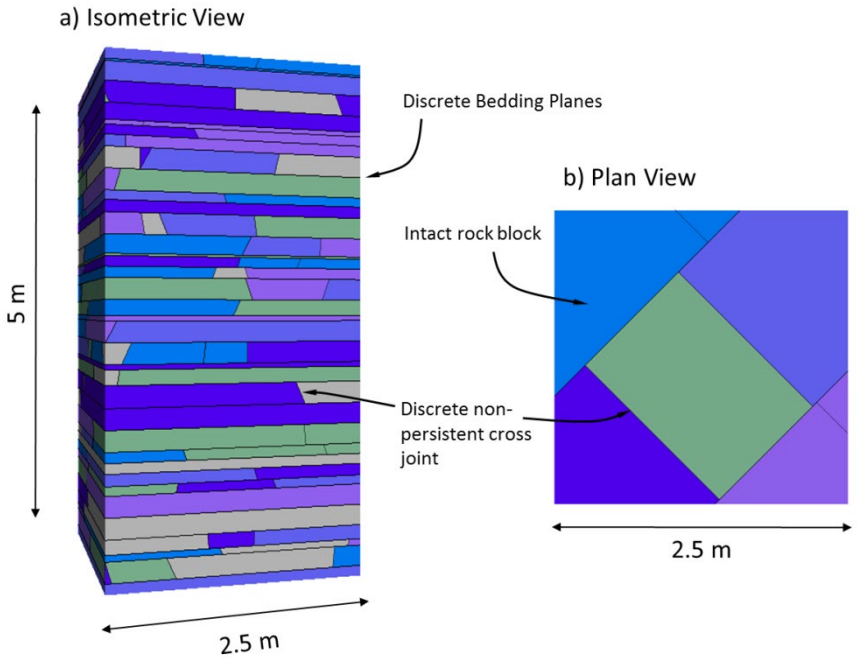

Figure 6 **3DEC model geometry used to simulate representative elemental LFWS specimen**

To account for the significant impact that micro-flaws (pores, open cracks, veins) and weathering/alteration can have on the strength scale effect, the rock block strength was assigned to be 50% of the σ_{ci} presented in Table 1. This value is based on an empirical scale effect relation for intact rock developed by Hoek and Brown (1980) and extended by Yoshinaka *et al.,* (2008). The joint cohesion and friction angles were assigned consistent with the values presented in Table 2.

Figure 7 illustrates the UCS stress-strain response of the LFWS material with β angles of 90° and 45°. Loading parallel to bedding (β = 90°) results in a stiff, brittle response as shear failure causes buckling of the intact rock blocks. Sliding along the discrete bedding planes at a β angle of 45° results in a weak, ductile loading response.

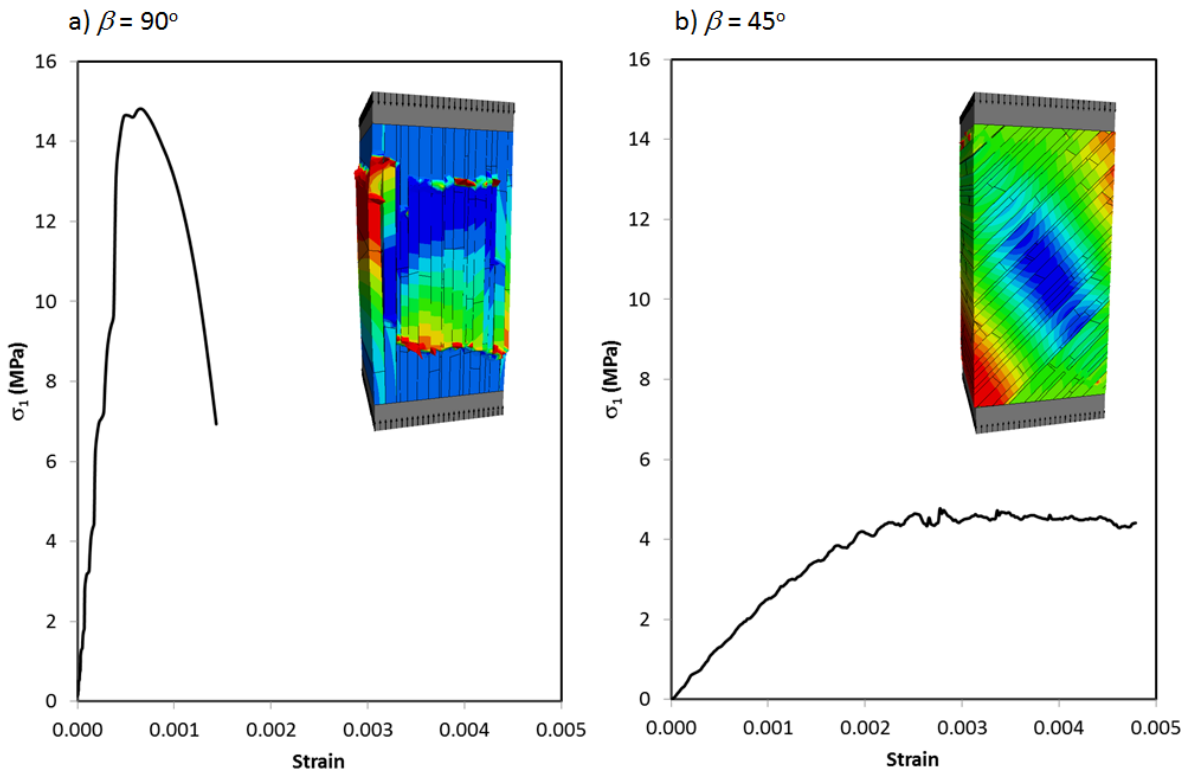

Figure 7 **UCS stress – strain response of LFWS domain at β angles of 90° and 45°**

In order to develop anisotropic rock mass strengths, a series of UCS and triaxial (σ_3 = 2 MPa) tests were simulated with β angles from 0° to 90°. Figure 8 illustrates the resulting U-shaped anisotropic strength curve with continuous variability for the LFWS material.

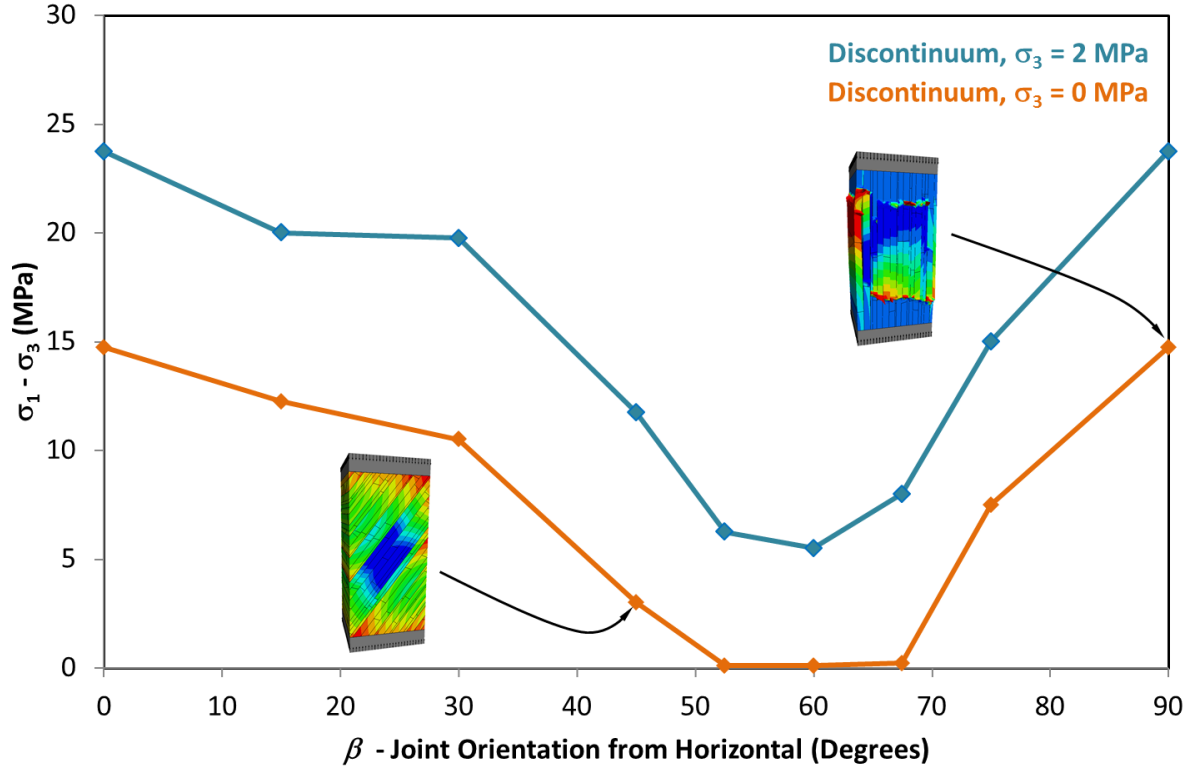

Figure 8 **U-shaped anisotropic strength curve with continuous variability for the simulated LFWS material**

5.2. Calibration of Anisotropic Strength and Deformation with UJRM Continuum Model

The Ubiquitous Joint and Subiquitous constitutive models require careful calibration of the matrix and ubiquitous-joint parameters to provide meaningful modelling results. Sainsbury and Sainsbury (2015) provide a discussion on the practical use Ubiquitous Joint models and highlight the misleading results that can be obtained when rock block and joint properties for an anisotropic rock mass are used directly for the matrix and ubiquitous-joint input parameters.

In order to derive Subiquitous material properties for the LFWS and UFWS Domains, the same testing procedure described in Section 5.1 was conducted in the three-dimensional finite difference code *FLAC*^{3D} (Itasca, 2015). Assumptions used in the calibration procedure include:

- The results of the discontinuum analyses accurately quantify the rock mass anisotropic behavior.
- The actual bedding plane cohesion and friction angle must be used to describe the peak ubiquitous-joint strength to provide a close match to the shear strength of the rock mass under planar sliding conditions.
- The matrix strength and deformation response must be calibrated to help compensate for the lack of length scale and stiffness parameters in the ubiquitous-joint formulation.

Within the UJRM samples 5% of the ubiquitous joints were rotated to be orthogonal to the dominant joint/bedding fabric. Sainsbury and Sainsbury (2015) found that the inclusion of orthogonal ubiquitous joints promotes continuously variable strength with increasing β angles, and also introduces some bending resistance within the ubiquitous joint system.

A series of UCS and triaxial (σ_3 = 2 MPa) tests were simulated for the UJRM materials with β angles from 0° to 90° to confirm the calibrated response. Figure 9 illustrates the resulting U-shaped strength curve for the LFWS UJRM material, together with the results from the discontinuum simulations.

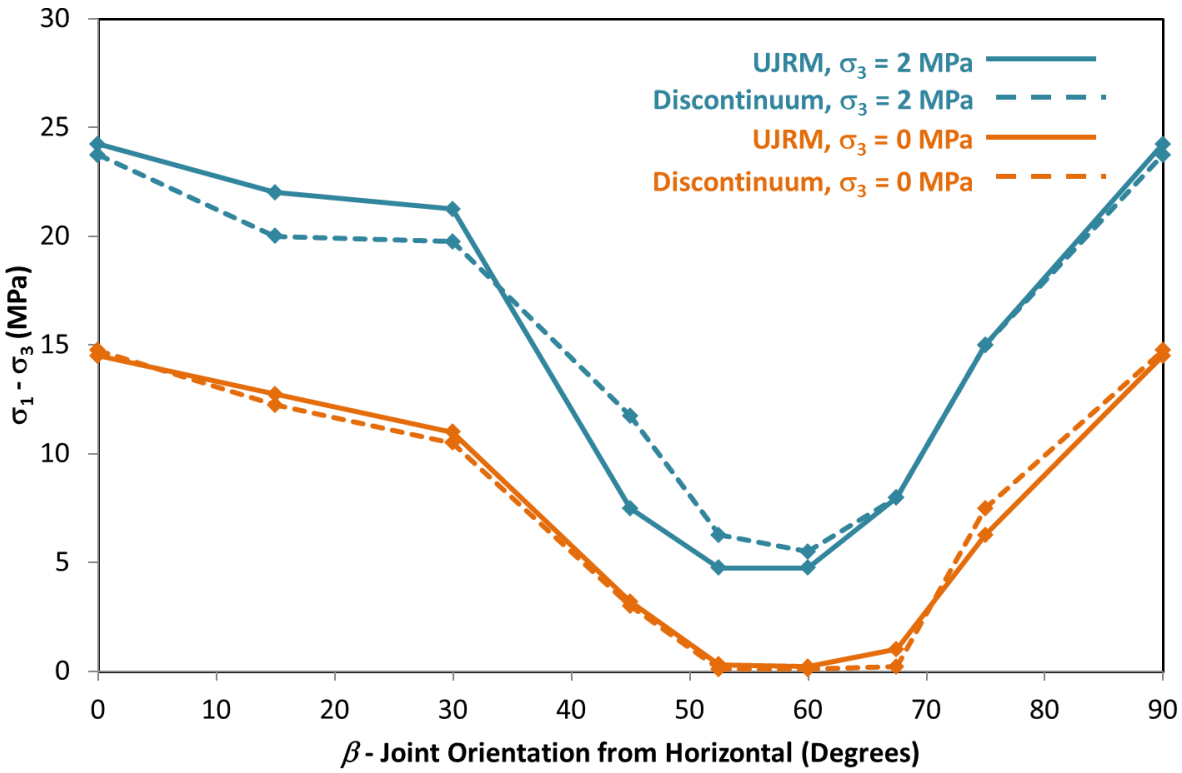

Figure 9 **Calibrated UJRM anisotropic strength response compared to the discontinuum anisotropic response for the LFWS material**

The calibrated UJRM input properties for the UFWS and LFWS domains are presented in Table 3. A detailed discussion on the UJRM calibration procedure, matrix and joint softening is provided in Sainsbury and Sainsbury (2013).

Table 3 Calibrated UJRM input properties used to simulate the UFWS and LFWS domains

	LFWS	UFWS
Rock Mass		
UCS (MPa)	30	39
GSI	60	60
mi	6	6
Matrix		
UCS (MPa)	15	19.5
GSI	100	100
mi	6	6
Modulus (GPa)	20.4	20.4
Cohesion (MPa)	2.8	5.3
Tension (kPa)	280	530
Friction (Deg.)	46	49
Joint		
Cohesion (kPa)	80	88
Friction (Deg.)	28	27

5.3. Analysis of UJRM Material Response

The response of the LFWS UJRM has been further explored to demonstrate the strength and deformation response of the UJRM material under various simulated stress paths. Figure 10a illustrates the stress-strain response of the LFWS UJRM material when all of the ubiquitous joints have been randomly oriented. The peak strength of this material provides a close match to the Hoek-Brown failure envelope derived from the rock mass GSI, UCS and m_i parameters (presented in Table 1). This provides confidence that the combination of matrix and ubiquitous joint properties in the simulated UJRM material is consistent with well-established empirical strength estimation techniques for isotropic rock masses.

Figure 10b illustrates the strength of the UJRM material from simulations that represent uniformly oriented joints at rotated β angles. The UJRM material is strongest when loaded perpendicular to the bedding orientation and weakest when loaded at an angle of approximately 60° (measured clockwise from horizontal). The variation in anisotropic response is also presented where the upper and lower peak strengths are compared to the Hoek-Brown failure envelope derived from the GSI, UCS and m_i parameters.

When a simulated direct shear test is conducted with a loading direction parallel to the bedding, the resulting shear strength of the UJRM material provides a close match to the adopted shear strength of the actual bedding planes, as illustrated in Figure 10c.

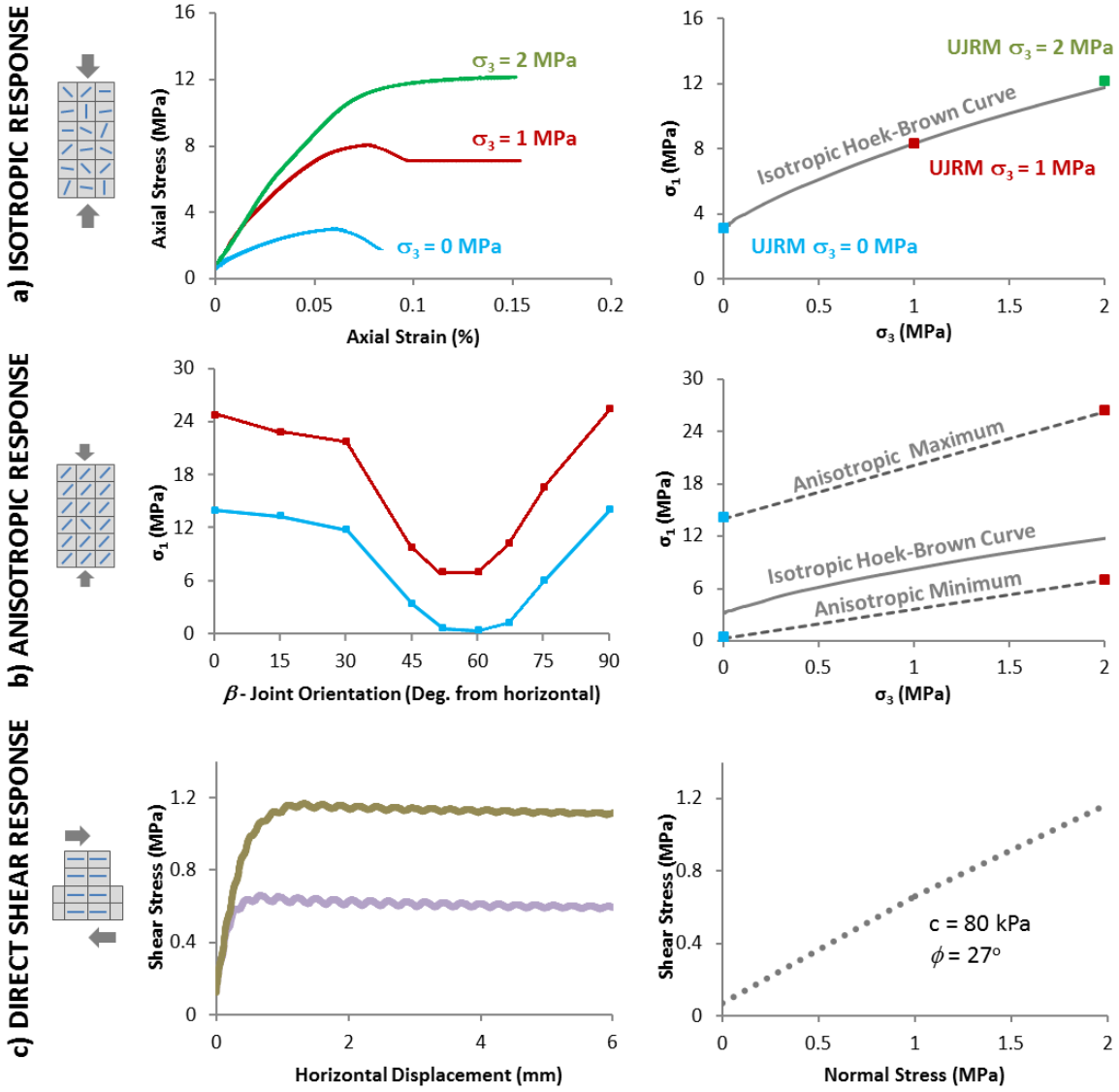

Figure 10 **Calibrated continuum responses Lower Footwall Shale**

6. Analysis of the Stage 8 Cutback Instability

6.1. Stage 8 Cutback Model Geometry and Construction

A three-dimensional *FLAC*^{3D} model was constructed to simulate the Stage 8 Cutback. Six geological discontinuities have been simulated as discrete interfaces within the model. Figure 11 illustrates the distribution of the geotechnical domains throughout the model, together with the discrete structures (interfaces). The Page Creek Fault was simulated as a 10 m thick weak zone between two discrete interfaces. A phreatic surface was assumed approximately 25 m behind the pit face.

The model geometry was constructed with the solid modelling package Rhinoceros (McNeel and Associates, 2015) and the mesh generation component of Abaqus/CAE (Dassault Systèmes, 2015). It is important to construct high quality, near unit aspect ratio model elements (zones) to ensure numerical stability within the complex array of intersecting interfaces that simulate the discrete large-scale structures.

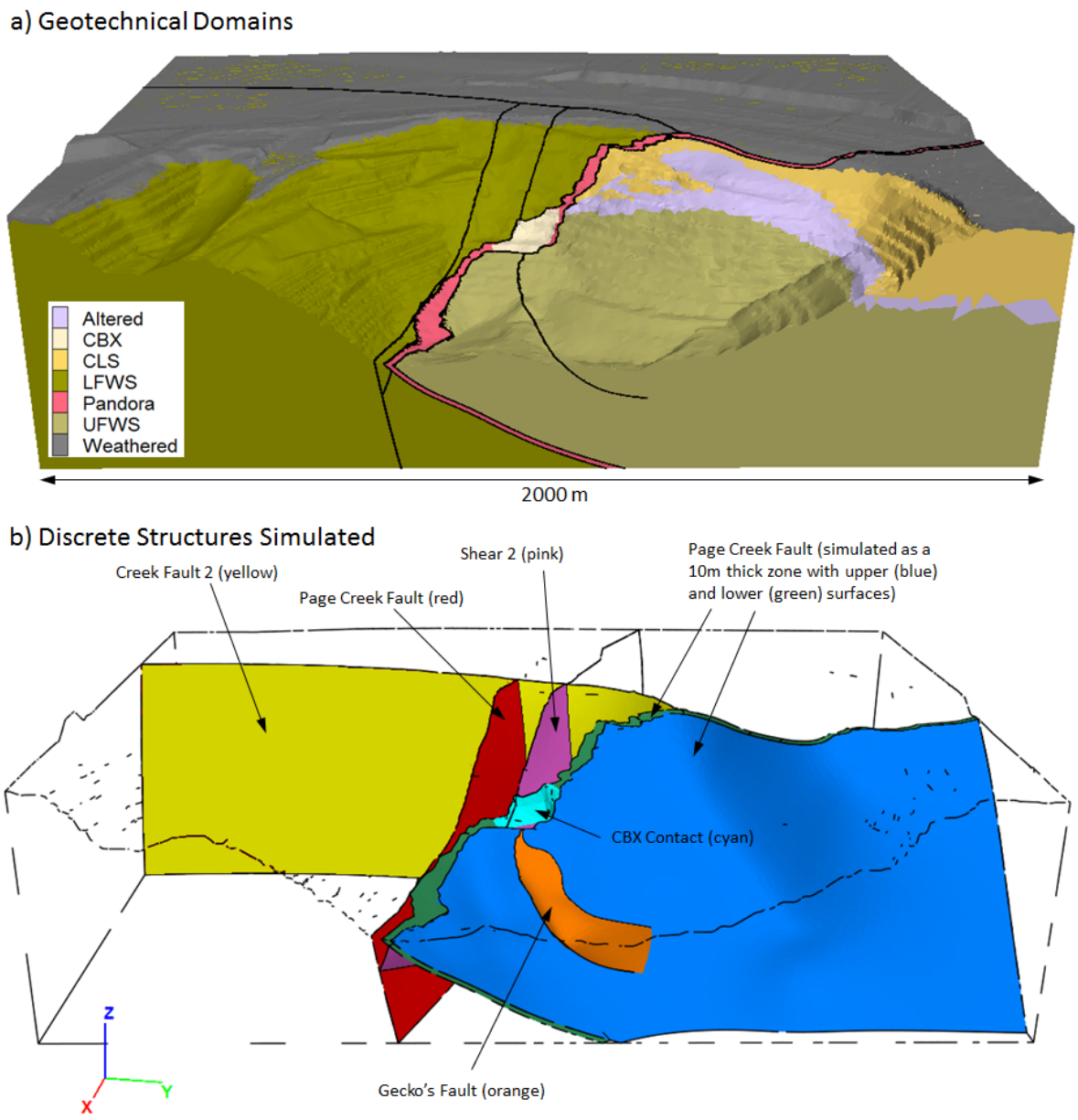

Figure 11 Geotechnical domains simulated within the model

The orientation of the bedding fabric within the LFWS and UFWS Domains was assigned based upon available face mapping and drill core information. Figure 12 illustrates the bedding fabric (ubiquitous joint) orientations assigned within the model. The unfavourable bedding orientation within the LFWS Domain is clearly observed.

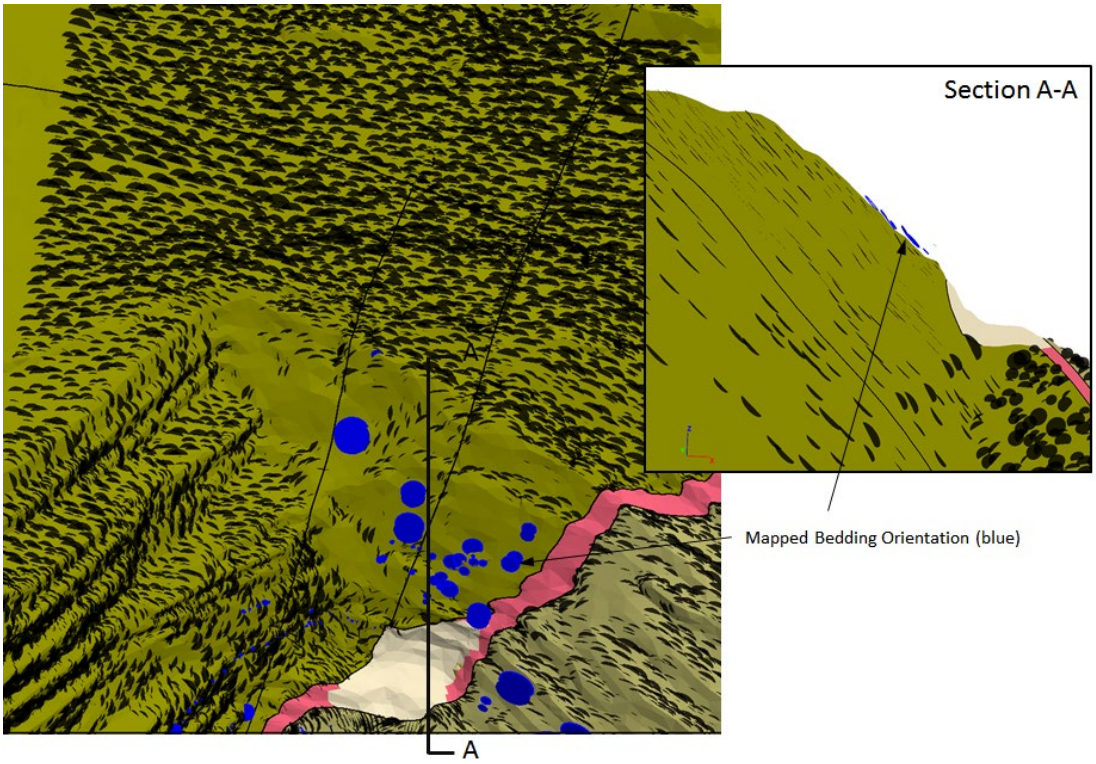

Figure 12 Bedding fabric (ubiquitous joint) orientation within LFWS and UFWS Domains

6.2. Simulation of Isotropic Rock Mass Conditions

Separate stability analyses have been performed assuming isotropic and anisotropic rock mass conditions. The isotropic modelling results provide a basic understanding of the slope stability that can be directly compared to other conventional pit slope analysis methods.

A bi-linear, Mohr-Coulomb, strain-softening constitutive model was used to simulate the isotropic behaviour of the rock mass domains. The shear strength of the geotechnical domains were estimated by fitting a bilinear Mohr-Coulomb envelope to the non-linear Hoek-Brown curve derived from the properties presented in Table 1. Figure 13a illustrates the predicted slope displacement after excavation of the entire Stage 8 Cutback. An alternate isotropic analysis was conducted using the UJRM model by providing a random orientation to each ubiquitous joint, as illustrated in Figure 13b.

Total displacement has been used to show the relative magnitudes in different areas of the pit during the simulation of mining. These displacements are not only associated with the movements that are expected to occur towards the excavation, but also include some component of uplift that occurs as the weight of the excavated rock is removed. Areas with displacement greater than 1 m provide an indication of areas of the pit slope where progressive failure is occurring.

Both isotropic modelling approaches result in a similar unloading deformation reposnse for the Stage 8 Cutback which provides confidence in the elastic response of the UJRM modelling approach. However, apart from minor instability (displacement > 1m) associated with Pandora's Fault, neither analysis represents the observed instability within the LFWS material.

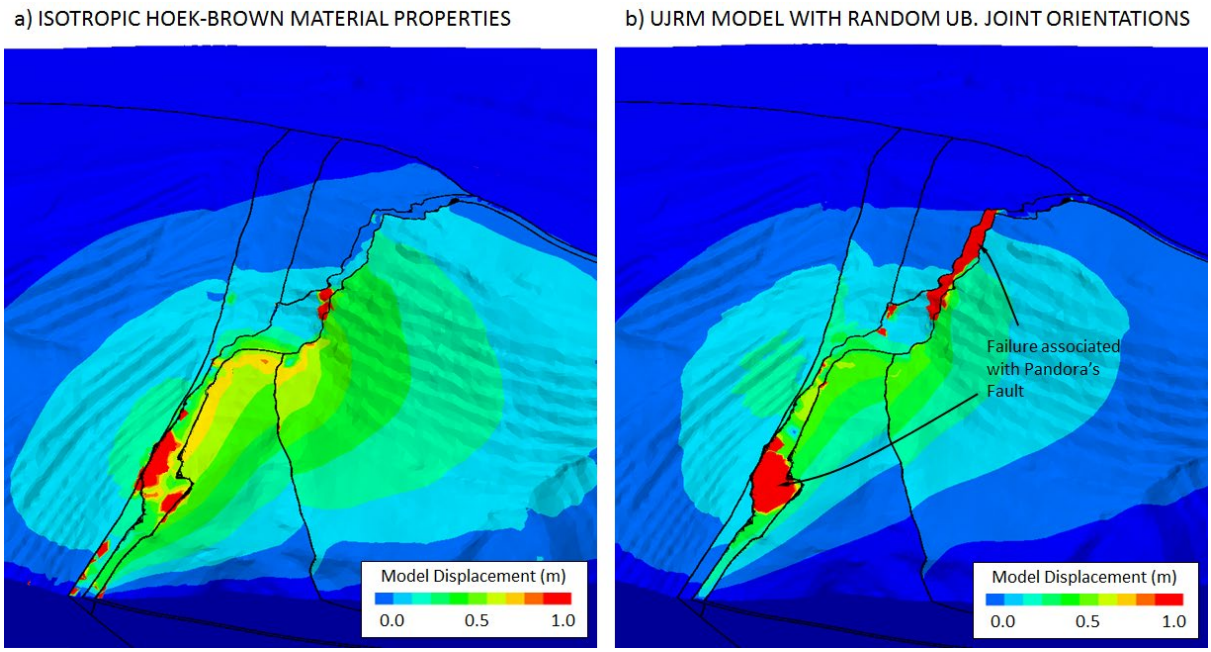

Figure 13 Simulated model displacement with isotropic material properties

6.3. Simulation of Anisotropic Rock Mass Conditions

The UJRM material developed for each of the LFWS and UFWS domains, together with the *in situ* bedding fabric orientation provides an accurate representation of the anisotropic slope behaviour. Figure 14a illustrates the total displacement after excavation of the Stage 8 Cutback. Significant displacement (> 1 m) is predicted within the weak Pandora's Fault material and the LFWS material above the CBX Domain. The model displacement provides a close match to the measured prism displacements presented in Figure 4.

Model velocity (m/step) is a metric used in numerical analyses to determine whether an area in the model is either stable or undergoing active plastic deformation. A model velocity of $1e^{-6}$ m/step indicates stability in the finite-difference calculation. Figure 14b illustrates the model velocity at the completion of the simulation. Although active progressive failure (> 1e-6) is only predicted in the weak Pandora's fault material, elevated model velocities in the LFWS material between the Page Creek and Pandora's Fault, which indicates an ongoing creep type response.

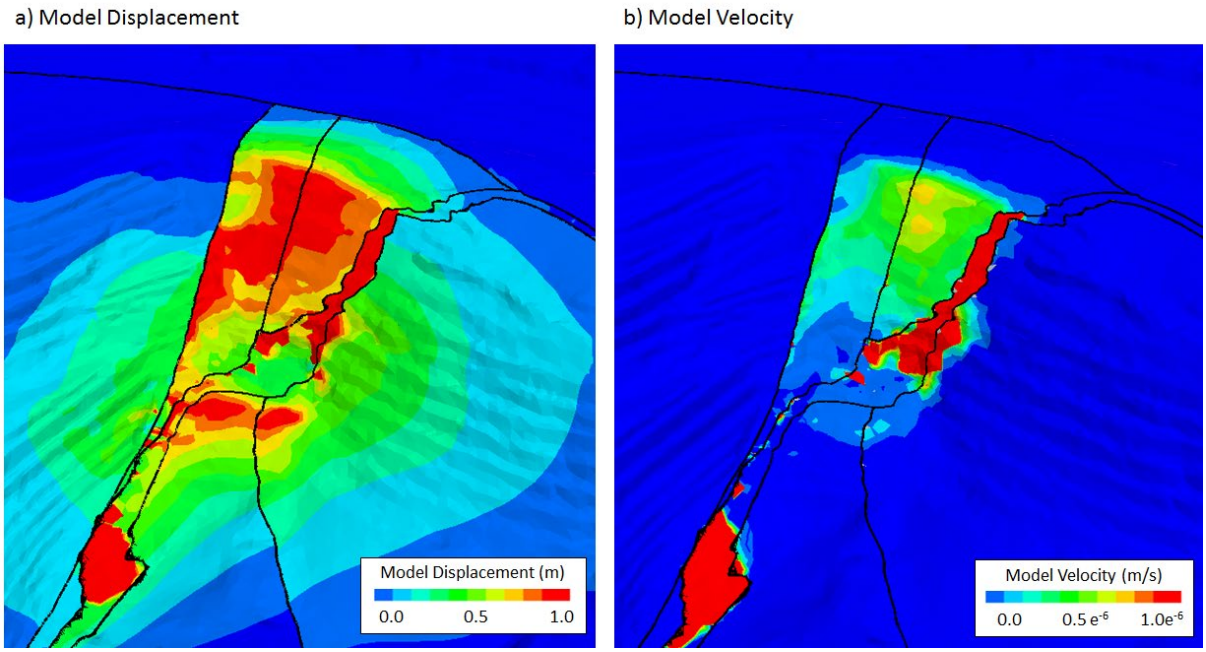

Figure 14 Model displacement and velocity after excavation of the Stage 8 Cutback

Figure 15 provides a section through the unstable zone in the model that presents model displacement and failure states. The primary failure mechanism is predicted to be shear failure along bedding (u:shear) in the LFWS. The gradual softening of the bedding joint cohesion behind the pit face is consistent with creep behaviour.

The model provides a good match to the observed rotational behaviour of the CBX Domain. Figure 16 illustrates a cross-section of displacement through the CBX Domain. The buttressing effect of the strong, massive material can clearly be observed. The simulated rotational response of the upper section of the unit compares well with the observed *in situ* response.

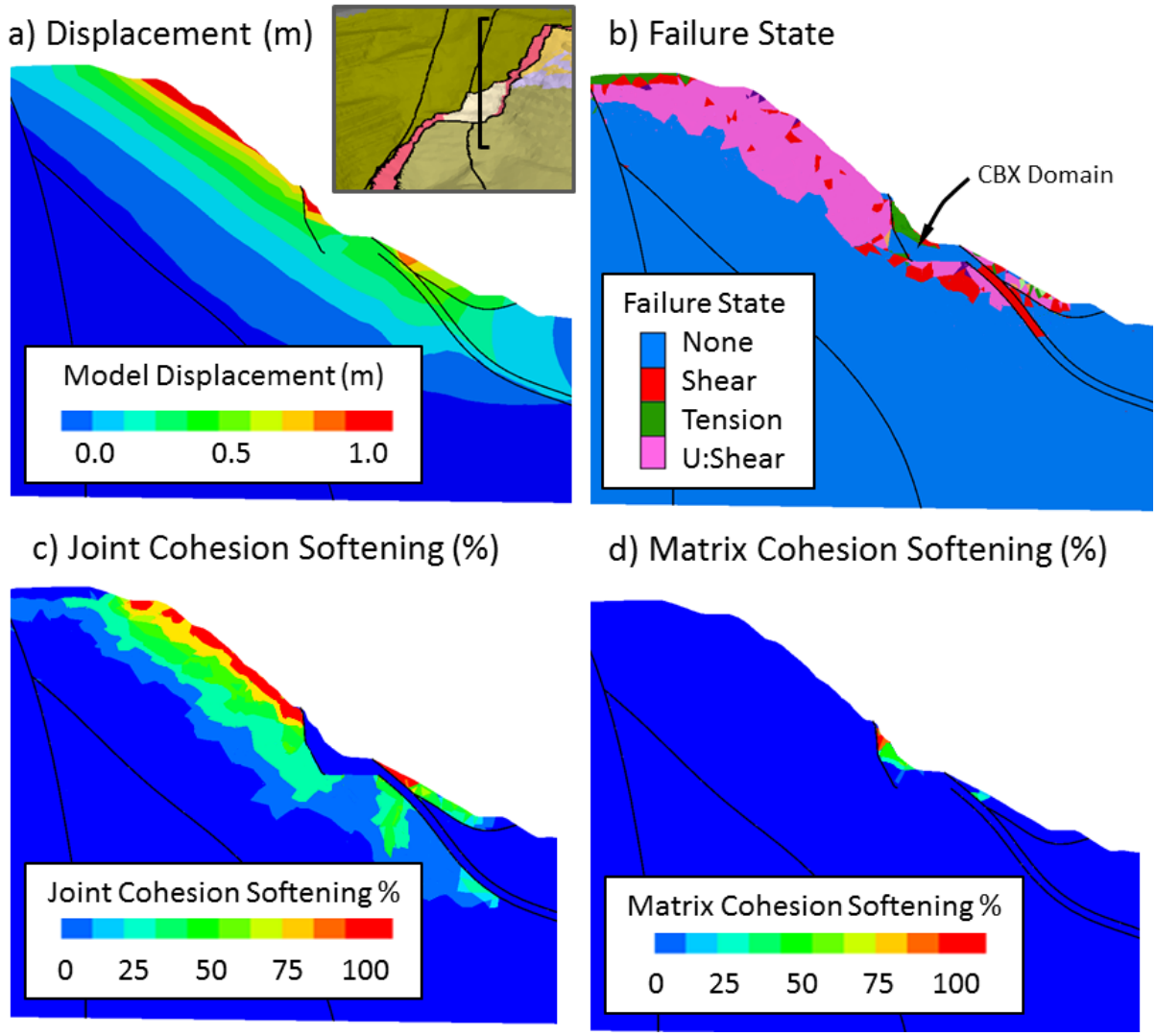

Figure 15 **Model response presented on a section through the Stage 8 Cutback**

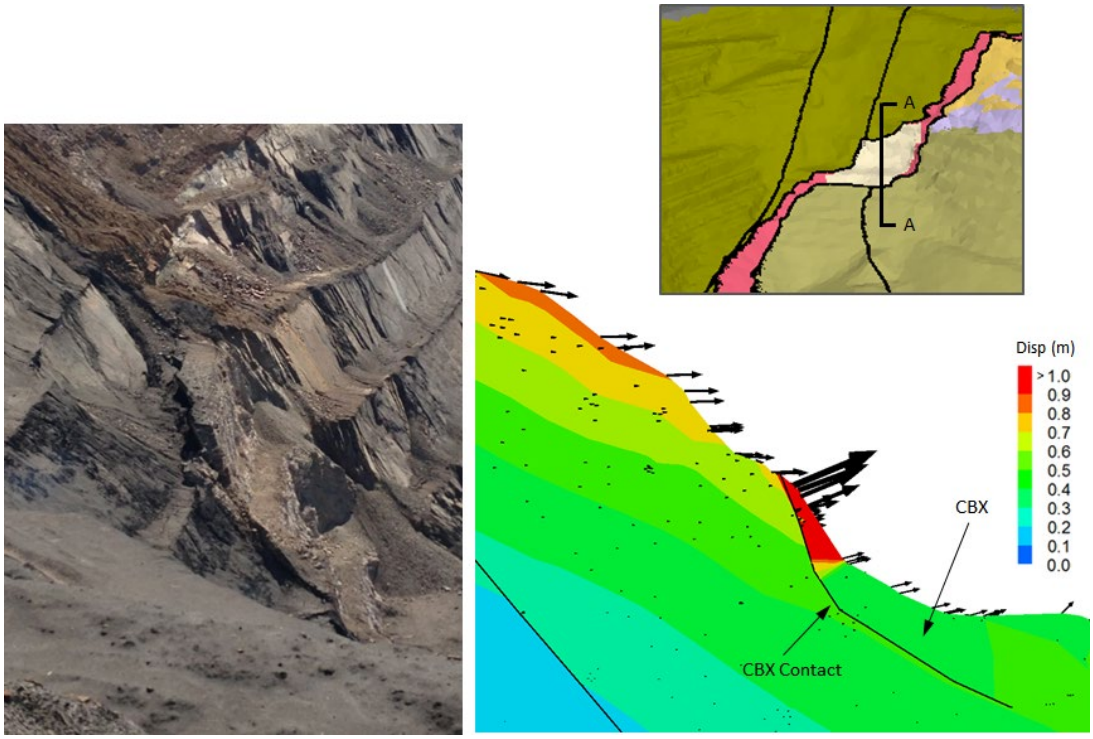

Figure 16 Observed and modelled rotation of CBX Domain

A total strain criterion of 0.005 (0.5%) has been used to assess the limit of large-scale surface cracking expected behind the crest of the Stage 8 Cutback. This total strain criterion has been used to calibrate the limit of large scale fracturing at the Kiruna, Grace and El Teniente Mines (Sainsbury and Stockel, 2012; Sainsbury *et al.*, 2010 and Cavieres *et al*., 2003).

Figure 17 illustrates the total strain predicted after excavation of the Stage 8 Cutback. The area in red indicates total strain greater than 0.005 (0.5%) which is likely to cause large-scale cracking of the rock mass. The simulated limit of large-scale cracking provides a close match to the location and orientation of the observed tension cracks.

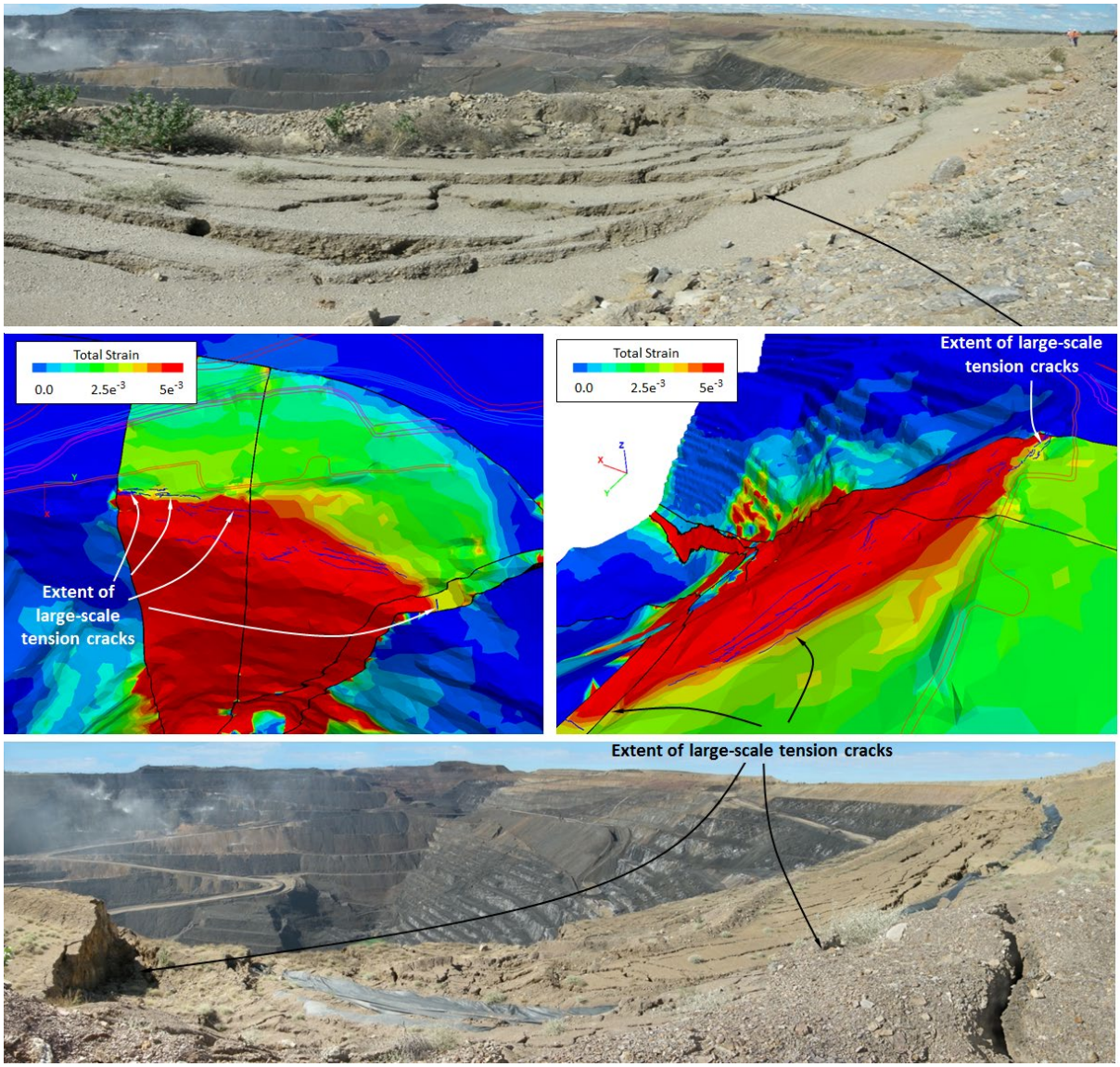

Figure 17 **Current assessment of total strain (red contour = limit of large-scale cracking)**

7. Conclusions

Three-dimensional numerical analyses of complex anisotropic slope instability at the Century Mine have been conducted to assist mine personnel implement a slope management plan that allowed successful recovery of 1.8 millions of tonnes ore beneath a transitional slope failure mechanism.

Simulation of the anisotropic strength and deformation behaviour of the rock mass materials with the UJRM modelling technique provides an accurate representation of the true behaviour of the complex failure mechanism and eliminates several uncertainties and assumptions associated with conventional isotropic and two-dimensional slope stability analysis methods.

The modelling results provide a close match to the monitored and observed behaviour of the complex Stage 8 Cutback failure mechanism.

8. Acknowledgements

The authors gratefully acknowledge the permission of management at the MMG Century Mine for permission to publish this work.

9. References

Barton, N. (1973) Review of a new shear strength criterion for rock joints, Engineering Geology, Elsevier, Amsterdam, Vol. 7, pp. 287-332

Barton, N. (1976) The shear strength of rock and rock joints. Int. Jour. Rock Mech. Min. Sci. and Geomech. Abstr., Vol. 13, No. 9: 255-279.

Broadbent, C.D and Zavodni, Z.M (1982). Influence of rock structure on stability. Stability in Surface Mining, Volume 3, Society of Mining Engineers, Chapter 2.

Broadbent, G. C., Andrews, S. J. and Kelso, I. J. (2002) A decade of new ideas: geology and exploration history of the Century Zn-Pb-Ag deposit, northwestern Queensland, Australia. Special Publication-Society of Economic Geologists, 9, 119-140.

Cai, M., Kaiser, P.K., Tasaka, Y. and Minami, M., (2007) Determination of residual strength parameters of jointed rock masses using the GSI system. International Journal of Rock Mechanics and Mining Sciences, 44, p. 247-265

Cavieres, P., Gaete, S. Lorig, L. and Gomez, P. (2003) Three-dimensional analysis of fracturing limits induced by large scale underground mining at El Teniente Mine, in 'Soil and rock America 2003, (ed. P. J. Culligan et al.), 893–900; 2003, Essen, Verlag Glu¨ckauf.

Clark, I.H. (2006) Simulation of Rock mass Strength Using Ubiquitous Joints. In: R. Hart and P. Varona (eds), Numerical Modeling in Geomechanics — 2006; Proc. 4th International FLAC Symposium, Madrid, May 2006. Paper No. 08-07, Minneapolis: Itasca.

Goodman, R.E. (1967) Analysis of Structures in Rock – Research on Rock Bolt Reinforcement and Integral Lined Tunnels. Omaha District, Corps of Engineers, Nebraska. Technical Report Number 3.

Halim, I.S., Chen, W-P. and Ilsley, R. (2008) Initial Support Design for Tunnels in Horizontally Bedded Sedimentary Rock. North American Tunneling: Proceedings of the North American Tunneling Conference, San Francisco. SME

Hendersonhall, B. D., Lucas, D., Kerr, N. & Pennisi, C. (2010) Practical Management of Progressive Large Failures at Minerals and Metals Group Century Mine. Seventh Large Open Pit Mining Conference. Perth, W.A.

Itasca Consulting Group (2015) Fast Lagrangian Analysis of Continua in Three-Dimensions Version 5.0

Itasca Consulting Group (2015) 3-Dimensional Distinct Element Code. Version 5.0

Hoek, E. 1964. Fracture of anisotropic rock. *J.S. Afr. Inst. Min. Metall*. **64**, No. 10, 501-518.

Hoek, E. and Brown E.T. (1980) Underground Excavations in Rock. London: Institution of Mining and Metallurgy. 527 pages

Jaeger, J.C. 1960. Shear failure of anisotropic rocks. Geol Mag. 97, p. 65-72.

Kazakidis, V. and Diederichs, M. 1993. Understanding Jointed Rock Mass Behaviour Using a Ubiquitous Joint Approach. Int. Journal Rock Mechanics Mineral Science & Geomechanics Abstracts Vol. 30, No. 2, pp. 163-172, 1993.

Kurucuk, N. and Sweeney, E. (2012) Slope Stability Assessment Century. Proceedings of the 9th Australia - New Zealand Young Geotechnical Professionals Conference, Melbourne, Australia, 2012.

McLamore, R. and Gray, K.E. (1967) The mechanical behaviour of anisotropic sedimentary rocks. Journal of Energy for Industry, Trans. Am. Soc. Mech. Engrs Ser. B, 89: 62-73.

Nasseri, M.H.B., Rao, K.S. and Ramamurthy T. (2002) Anisotropic strength and deformational behaviour of Himalayan schists. International Journal of Rock Mechanics and Mining Sciences, Volume 40, Issue 1, January 2003, Pages 3–23.

Ramamurthy, T. (1993) Strength, modulus responses of anisotropic rocks. In: Hudson J.A., (ed.). Compressive rock engineering, Vol. 1. Oxford: Pergamon, 1993. pp. 313–29.

Sainsbury, B., Pierce, M. and Mas Ivars, D. (2008). Analysis of Caving Behavior Using a Synthetic Rock Mass (SRM) - Ubiquitous-joint Rock Mass (UJRM) Modelling Technique in the Proceedings of the 1st Southern Hemisphere International Rock Mechanics Symposium (SHIRMS), September, 2008.

Sainsbury, D. P., B. L. Sainsbury and L. L. Lorig. (2010) "Investigation of Caving Induced Subsidence at the Abandoned Grace Mine," Trans. IMM, Section A, Min. Tech., 119(3), 151-161, DOI: 10.1179/174328610X12820409992336.

Sainsbury, B. and Stockel, B-M. (2012) Large-scale caving and subsidence assessment at the Kiirunavaara Lake Orebody. MassMin 2012, Sudbury, CA.

Sainsbury, D. and Sainsbury, B. (2013) Three-Dimensional Analysis of Pit Slope Stability in Anisotropic Rock Masses. Proceedings of Slope Stability 2013. Brisbane, Australia. Australian Centre for Geomechanics, Perth

Salvoni, M., Abbott. K. and Dight, P.M. (2015) Improvement of pseudo-3D pit displacement map technique through geodetic prism data integration. FMGM 2015- 9th International Symposium on Field Measurements In Geomechanics, Australia, Sydney, 9 - 11 September 2015. Australian Centre for Geomechanics, Perth

Salvoni, M., Abbott. K. and Dight, P.M. (2015) Micro-seismic monitoring at MMG's Century Mine, Northwest Queensland. Proceedings of Slope Stability 2015. Cape Town, South Africa. SAIMM.

Stead, D. (2015) The influence of shales on slope stability, ISRM Congress, Shale Symposium, Montreal, 22pp.

Sweeney, E. and Abbott, K. (2015) Geotechnical Analyses for Risk Management of a Large Scale Failure at MMG's Century Mine, Northwest Queensland. Proceedings of Slope Stability 2015. Cape Town, South Africa. SAIMM.

Yoshinaka, R., Osada, M., Park, H., Sasaki, T. and Sasaki, K. (2008). Practical determination of mechanical design parameters of intact rock considering scale effect. Engineering Geology, 96, pp. 173-186.